ISSN 2321-807X
Volume 12 Number23
Journal of Advances in chemistry

Multi-Stable Stochastic Resonance Based Protection Scheme for Parallel Transmission Lines with UPFC

Mary A.G. Ezhil[1], Joseph Jawhar S[2], Chellaswamy C[3]
[1,2]*Department of Electrical and Electronics Engineering, Arunachala College of Engineering for women, Tamilnadu, India.*
e.mail:[1]maryezhil1981@rediffmail.com
[2]*Principal, Arunachala College of Engineering for women, Tamilnadu, India.*
e.mail: [2]profjosephjawhar@gmail.com
Department of Electronics and Communication Engineering, Rajalakshmi Institute of Technology, Chennai, Indvia.
E.mail: chella_info@yahoo.co.in

ABSTRACT

This paper presents a multi-stable stochastic resonance (MSR) based on complex wavelet transform (CWT) for protecting a double line transmission system with unified power flow controller (UPFC) in one line. The fault detection at the sending end is recognized by the collective sum technique (CST) using the current signals of all the three-phases with heavy background noise. The noisy signal is processed by parameter compensation and the processed signal is decomposed by CWT with different scale frequencies. The spectral energies of each phase can be used to identify the faulty phases. The CWT is used to compute the spectral energies of each phase current. The proposed scheme has been studied for wide variation of operating parameters and compared with two other fault extraction methods such as EMD-based spectral analysis and wavelet transform with post spectral analysis. The test results of the proposed CWT based MSR algorithm indicates that it can accurately detect and classify the fault with in one cycle from fault inception.

Indexing terms/Keywords

complex wavelet transform, unified power flow controller, collective sum technique, spectral energy, double line transmission system, multi-scale stochastic resonance

Academic Discipline And Sub-Disciplines

Electrical and Electronics Engineering, Power Electoronics.

SUBJECT CLASSIFICATION

Power System.

TYPE (METHOD/APPROACH)

Sumulilan setup and output was verified.

INTRODUCTION

There is an enormous increase in power transaction due to power system renovation and different factors such as environmental, right-of-way and high cost, which forms the hurdle for the expansion of power transmission network. With the advancement in flexible AC transmission system (FACTS), several innovative concepts turn the system into more flexible and have control over power flow without altering the generation schedule. Optimal location identification and allocation of FACT devices improve various parameters of the system [1, 2]. FACTS controllers play an important role to control the power flow in a multi area power system. UPFC is one of the most versatile FACTS controller connected in series with the transmission line to control the power flow [3]. Various FACT tools has been used for this purpose such as static Var compensator (SVC), static synchronous compensator (STATCOM), static synchronous series compensator (SSSC), thyristor controller series capacitor (TCSC), unified power flow controller (UPFC) and interline power flow controller (IPFC) [4]. UPFC is one of the FACT tools which are used to manage the power flow by inserting active and reactive components in series with the line [5]. Optimal location and modeling of UPFC enhance the static voltage stability [6, 7].

A new current-based model has been developed for IPFC by Anton et.al with different load flow conditions. This model has been tested on IEEE standard test systems and this method produces faster convergence [8]. Optimal location identification and installation of FACT device is an investment constraint. Moreover, reliable and secure operation of power system is important under normal and contingency condition [9]. Wavelet transform is an efficient method in analyzing current and voltage signals at both the ends of transmission lines for calculating the fault index. The faults can be analyzed both in time and frequency domain and Haar wavelet is used to calculate the faulty phases [10]. Due to the fast growing digital communication techniques, it is possible to build up communication and digital protection schemes suitable for EHV transmission environment. The fault detection of transmission lines using wavelet based transient extraction has been studied in [11, 12]. Wavelet based multi resolution analysis is introduced by Usama et al. for transmission lines fault location [13]. For increasing the accuracy of transmission lines fault location, GPS based algorithm has been proposed in [14].

Another detection method including noise is stochastic resonance method. The concept of MSR has been introduced by Benzi et al. in 1981 and it is widely used in signal processing, physics, and fault diagnosis in different fields [15]. In contrast, to increase the signal-to-noise ratio (SNR), MSR utilizes noise instead of eliminating. In recent years, MSR has been widely used in the field of signal processing because of its capability of weak signal detection [16]. Many literatures have been proposed for identifying single-frequency signals with noise. In real applications, the signal is mixture of both the low and high frequencies. The high frequency signal components are converted into low frequency components by scaling [17]. A new method has been introduced by Tao et al. for weak signal detection stochastic resonance using single-well method [18]. This method utilizes only one adjustable parameter and makes the system to reach optimum state. The majority of existing methods are based on bisatble or monostable for detecting multi-frequency. When SNR is very low, the bistable and monostable stochastic resonance method cannot detect the signals perfectly. Hence, multi-stable stochastic resonance method is used in this paper for more accurate results. On the other hand, no reports are found on multi-frequency using multi-stable stochastic resonance method on parallel transmission line faults.

In this paper, a novel CWT based MSR algorithm is presented to detect and classify the faults on transmission system including UPFC. The detection method is based on complex wavelet transform and parameter compensation to produce a multi-stable stochastic resonance scheme is proposed. The remnants of this paper is organized in the following ways: section 2 describes the wavelet transform with decomposition and multi-frequency signal detection based on parameter compensation for multi-stable stochastic resonant; section 3 describes CST based cross-disparity protection scheme; section 4 explains the simulation results and discussions; and finally, conclusion is summarized in section 5.

2. FORMULATION OF MSR BASED CWT

2.1 Multi-stable SR model

The multi-stable SR is a multi-stable non-linear system which is driven by periodic signals and white noise. It is used to identify the weak signals by transferring noise energy into useful signals that resonate. The Langevin equation can be written as [19]:

$$\frac{dx}{dt} = -\frac{du}{dt} + A_0 \sin(\omega_0 + \varphi) + n(t) \quad (1)$$

where A_0 is the amplitude of periodic amplitude, f_0 is the driving frequency, ϕ is the phase. $n(t) = \sqrt{2D}g(t)$, $\omega = 2\pi f$, where D represents the noise intensity and g(t) represents the Gaussian white noise with zero mean and unit variance. For the multi-stable model the potential function u(x) can be expressed as [20]:

$$u(x) = \frac{x^6}{6a'} - \frac{(1+c)x^4}{4b'} + \frac{cx^2}{2} \quad (2)$$

where a', b', and c are the barrier parameter of the multi-stable potential and it has the values, a'=20+5c (0<c<1); b'=5, c>0; a=27.5-2.5c (1<c<3). The above equation has three stable and two unstable solutions. Now equation (1) can be written as:

$$\frac{dx}{dt} = M\left[-\frac{x^5}{a} + \frac{(1+c)x^3}{b} - cx + \sum_{k=1}^{n} A_k \sin(\omega_k t) + \sqrt{2D}g(t)\right] \quad (3)$$

The system is more stable at the lowest points and the potential energy is minimum when $A_0 \sin(\omega_0 + \varphi) + \sqrt{2D}g(t) = 0$. The output state of the system only moves inside the potential well and the signal energy cannot overcome the blocking of the barrier when the input is a weak periodic signal. On the other hand, the noise energy is partially transferred to the signal for overcoming the barrier and to produce interaction when the input is noisy.

2.2 Parameter compensation for Multi-stable SR model

The traditional SR models mainly focus on low amplitude, low frequency, and low noise intensity [21]. To implement SR for high amplitude, high frequency, and strong noise intensity certain indirect method such as heterodyning, modulation, double sampling and parameter compensation are needed. Except parameter compensation, all the other method need to know the sampling frequency and the signal frequency, which is difficult for high frequency signals [22]. In this paper, parameter compensation is used to detect the fault and it can be obtained by integrating Eq. (3) and it can be expressed as:

$$x(t) = M\left\{\int\left[\frac{x^5}{a} + \frac{(1+c)x^3}{b} - cx + \sum_{k=1}^{n} A_k \sin(\omega_k t) + \sqrt{2D}g(t)\right]dt\right\}$$

$$= M\left\{\int\left[-\frac{x^5}{a} + \frac{(1+c)x^3}{b} - cx\right]dt + \int\left[\sum_{k=1}^{n} A_k \sin(\omega_k t)\right]dt + \int\sqrt{2D}g(t)dt\right\}$$

$$= M\left\{\int\left[-\frac{x^5}{a} + \frac{(1+c)x^3}{b} - cx\right]dt - \sum_{k=1}^{n}\frac{A_k}{2\pi f_k}\cos(\omega_k t) + \int\sqrt{2D}g(t)dt\right\} \quad (4)$$

From Eq. (4) one can easily understand that amplitude of input signal is reduced by $1/2\pi f_k$ after passing MSR system and the amplitude increases with increasing frequency.

2.3 MSR based on CWT

The wavelet transform offers simultaneous localization in time and frequency domain and computationally it is very fast in signal processing applications. The wavelet basis is a family of functions based on a mother wavelet R(t). It is a well-localized oscillating function and all other wavelet functions within the family are generated from translations and dilations of R(t). In fact, the R(t) has zero translation and a dilation of 1 and the generated equation is expressed as [23]:

$$\gamma_{a,b}(t) = \frac{1}{\sqrt{a}}\gamma\left(\frac{t-b}{a}\right), \mathrm{a} > 0 \quad (5)$$

where a and b are the dilation factor and frequency shift factor respectively. $\gamma_{a,b}(t)$ can be obtained from $\gamma(t)$ by dilation and translation. A family of functions can be obtained by changing a and b and the wavelet transform coefficient is given by

$$W_n(a,b) = \frac{1}{\sqrt{a}}\int x(t)\,\gamma^*\left(\frac{t-b}{a}\right)dt \quad (6)$$

The discrete wavelet can be obtained by taking $a=a_1^k$ and $b=a_1^k rb_1$ [24], and the corresponding wavelet function is $a_1^{-k/2}$ $\gamma(a_1^{-k}t - a_1^{-k}b)$, $k \in Z$. The discrete wavelet has discrete mode and it is binary; when $a_1=2$; we obtained $a=2^k$ and $b=2^k rb_1$, then the wavelet function is $2^{-k/2}$ $\gamma(2^{-k}t - rb_1)$, $k \in Z$. Subsequently, each transform coefficient is expressed as:

$$W_{Tn}(2^k, 2^k r) = 2^{-k/2}\sum_m \gamma^*\left(\frac{\mathrm{m}}{2^{\mathrm{k}}} - r\right)x(\mathrm{m}) \quad (7)$$

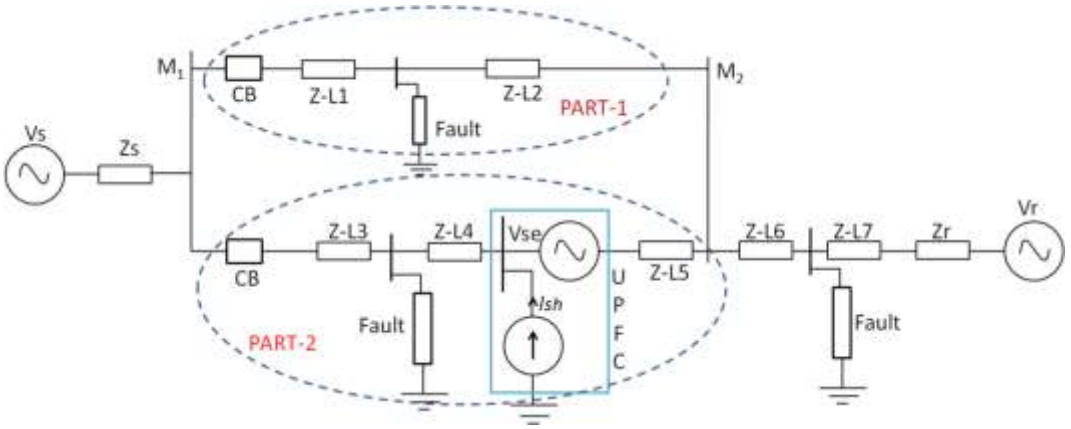

Figure 1. Connection of circuit breakers with location of fault.

Multi scale tuning is an effective method to obtain a preferable SR from the measured signal with multiple scales to be allocated in an approximate 1/*f* form. To enhance the response of SR system, 1/*f* noise is better than white noise [25, 26]. In this paper, Daubechies wavelet is chosen for decomposition and reconstruction of the arbitrary signal $f(t) \in L^2R$ and it can be expressed as

$$f(t) = \sum_k f_k(t) + \sum_k d_k(t)$$

$$= \sum_k \sum_m r_{k,m} \psi_{k,m}(t) + \sum_k \sum_m s_{k,m} \mu_{k,m}(t) \quad (8)$$

The optimal solution can be obtained by adjusting the tuning parameter, so that the arbitrary type signal noise can meet 1/f type.

3. PROPOSED PROTECTION METHOD

The proposed protection method with circuit breakers and location of fault is shown in Figure 1. It consists of two 210 kV, 1100 MVA substations with the transferring end impedance Zs, voltage Vs and the receiving end impedance Zr , voltage Vr respectively. The UPFC is located at the center of part-1. The phase difference (β) denotes the angle between the transferring and receiving end generating stations. The part-1 transmission line is divided into different subsections ZL-1, ZL-2.

3.1CST based cross-disparity Protection

There are three single phase relays, one for each phase has been located at the transferring end bus-A and the current transformers (CTs) are used to measure the currents in part-1 and part-2. The three relay units are used to protect the three phases of the two routes (part-1 and part-2) at the same time. CST based detection techniques has been used to detect the sharp changes in current and voltage of power system [27]. The CST based technique least affected by spikes, noise, and harmonics and it will not provide false detection during power swing and load switching [28] and it provides reliable protection to the system. It is because the difference between each phase current of part-1 and part-2 is larger than the set threshold of the system.

So the computation for the cross-disparity of the CST for a particular sampling instant n is given by

$$CV(n) = \left[CV(n-1) + \{S_{mes}(n) - S_{mes}(n-k)\}\right] \quad (9)$$

Where n represents the sampling instant, S_{mes} represents the measured phase current or voltage, CV is the computed CST value, and k represents the number of samples per cycles. Initially the length of CV will be zero and it starts with $(k+1)^{th}$ samples. The phase current of PART-1 with the threshold T_{H1} and the phase current of PART-2 with the threshold T_{H2} has the constraints: $|\mathrm{CV}(I_1)| - |\mathrm{CV}(I_2)| > \mathrm{S}_{\mathrm{TH1}}$ and $|\mathrm{CV}(I_2)| - |\mathrm{CV}(I_1)| > \mathrm{S}_{\mathrm{TH2}}$. Here two different thresholds (S_{TH1}, S_{TH2}) are needed because UPFC is included with part-2. The fault detection time by the proposed CST based cross-disparity Protection method is given as:

$$PD_R = \min(SP_{R,\text{PART-1}}, SP_{R,\text{PART-2}}) \quad (10)$$

$$PD_Y = \min(SP_{Y,\text{ PART-1}}, SP_{Y,\text{PART-2}}) \quad (11)$$

$$PD_B = \min(SP_{B,\text{PART-1}}, SP_{B,\text{PART-2}}) \quad (12)$$

Where PD represents the point of detection exists for each phase (phase-R, phase-Y, and phase-B) of part-1 and part-2; the index SP_R, part-1 represents the sample point at which the magnitude $\left(|\mathrm{CV}(I_{1,R})| - |\mathrm{CV}(I_{2,R})|\right)$ is equal or exceeds the threshold, and the index SP_R, part-2 represents the sample point at which the magnitude $\left(|\mathrm{CV}(I_{2,R})| - |\mathrm{CV}(I_{1,R})|\right)$ is equal or exceeds the threshold. The faulted circuit current for each phase reaches the threshold faster and the other point of detection PD_Y and PD_B can also be calculated in the similar manner.

3.2 Fault Classification

The CST may misdirect the process during the presence of noise or harmonic distortions. Therefore, the three phase current of both the lines must be analyzed for fault classification after the fault is detected. For that reason, one cycle (indicates one complete process) data of both the PART-1 and PART -2 has been taken and processed through CWT based MSR and the procedure for classifying the fault is as follows:

1) Find the detection point PD_R, PD_Y, and PD_B of three phases (both PART-1 and PART-2) and consider one cycle of data in which half cycle is from the left and the other from the right half of the detected point and then it is processed through CST.

2) The change of energy in the PD points are calculated separately for the two half cycles of the individual phase of two transmission lines PART-1 and PART-2. The resulting current can be represented in matrix form as:

$$Y_{R\times S} = \mathrm{CST}\left(\left[I\left(\mathrm{PD} - \frac{\mathrm{N}_s}{2}\right)\right]\right) \ldots I(PD) \ldots I\left(\mathrm{PD} - \frac{\mathrm{N}_s}{2}\right) \quad (13)$$

where $Y_{R\times S}$ is an (R×S) matrix, with N number of samples in the input signal and S is the S^{th} row of the CST matrix representing a particular frequency components of the input signal. I represent the current of each phase of PART-1 and PART-2. The resulting matrix has single R rows and S columns, which signifies the length of the signal.

3) The spectral energy content present in the input signal is calculated using (8) as:

$$E_{R\times S} = \left|Y_{R\times S}\right|^2 \tag{14}$$

The spectral energy is computed for individual phase current of each transmission lines. Number of frequency components is present in each sample. So the maximum spectral energy present in each column of (14) can be transformed in to a single column for each of S column. This can be formed as:

$$E_{PART,p} = E_{1\times S}^{\max} = \max\left(E_{R\times S}\right) \tag{15}$$

where the subscript PART and p represents the parallel lines, PART-1 or PART-2 (refer Figure 1) and the three phases R, Y, or r respectively. Now check the values of three matrices with the preset spectral energy (PSE). The faulted line can be easily identified if the value of matrix is greater than or equal to PSE. The control strategy is given by

if $(E_{1,R}- E_{2,R}) > S_{TH1}$, then fault on R_{PART-1}

else if $(E_{2,R}- E_{1,R}) > S_{TH2}$, then fault on R_{PART-2}

where R_{PART-1} indicates the phase-R of PART-1.

In this way the proposed MSR based on CWT classifies the fault at the end of one cycle of data and protect the system by issuing the trip signal. In addition to this the proposed scheme is able to determine single phase (LG), double phase (LLG), and three phase faults (3LG).

4. RESULTS AND DISCUSSION

The simulation was developed using MATLAB/Simulink R2014a in Intel core i5, 2.3 GHz with 6 GB RAM personal computer for the transmission system described in Figure 1. Number of simulation were carried out for various faults, by varying fault inception angle (β), fault locations (varying between 5% and 95% of the transmission lines), fault resistances (R_{fault}=5 to 200 Ω), UPFC series injected voltage phase angle (θ_{ser}), The angle difference between the transferring and receiving end voltage (α=40^o), and series injected voltage (V_{se} varying from 0 to 10% of the line voltage). A parallel transmission system (250 kV, 250-km) with 170-MVA UPFC installed in the midpoint of transmission line and the distance between M_1 - M_2 is 120 km. The sampling rate of 3.2 kHz, on a 50 Hz frequency has been chosen. The voltage sources inverters (VSIs) are connected through 2500 micro Farad common dc capacitances and the STATCOM part is connected through a 230/15 kV shunt transformer to the transmission system. In order to inject sinusoidal voltage, the SSSC part is connected to the power system through a 15/20 kV series transformer. The control system of UPFC with STATCOM and SSSC has been taken from [29]. The currents I_1 and I_2 are recovered for different fault conditions and the propose algorithm has been studied for different operating conditions of the UPFC.

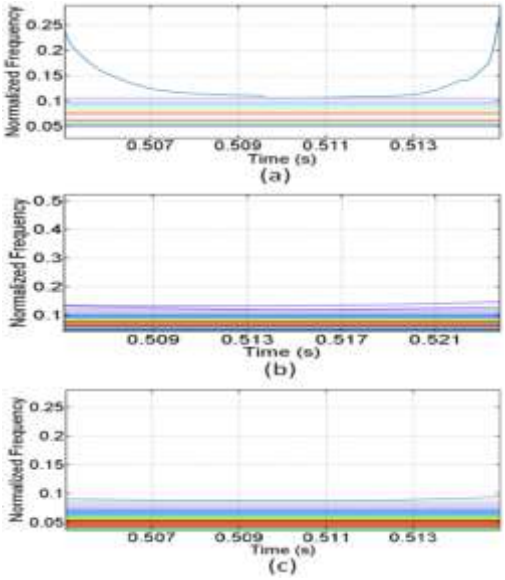

Figure 2. Spectral energy based fault classification on PART-2 for LLG fault (a) contour for phase-R current (b) contour for phase-Y current (c) contour for phase-B current.

4.1 Spectral Energy Based Fault Classification

In this scenario, the classification of LLG, LG, and 3LG fault for both the PART-1 and PART-2 has been considered. The spectral energies for each phase current of both the PART-1 and 2 can be calculated using the proposed CWT algorithm. To study different fault conditions, the fault starts at t=0.525 s and one cycle of current signal is used to calculate the spectral energies of all the three phases.

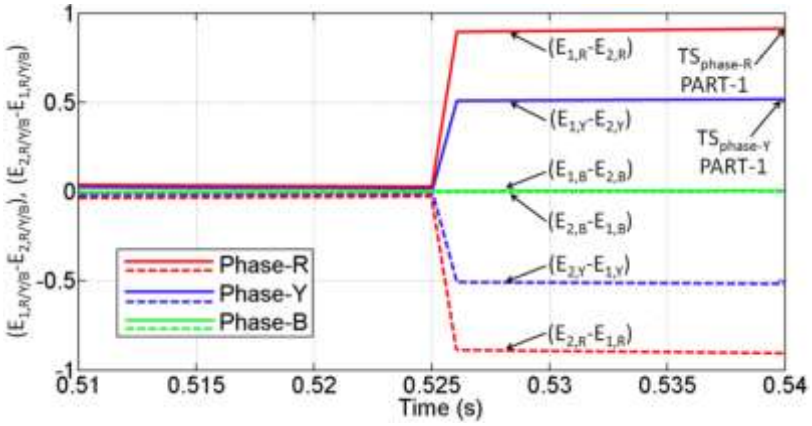

Figure 3. Fault classification using spectral energies for phase-R, phase-Y, and phase-B.

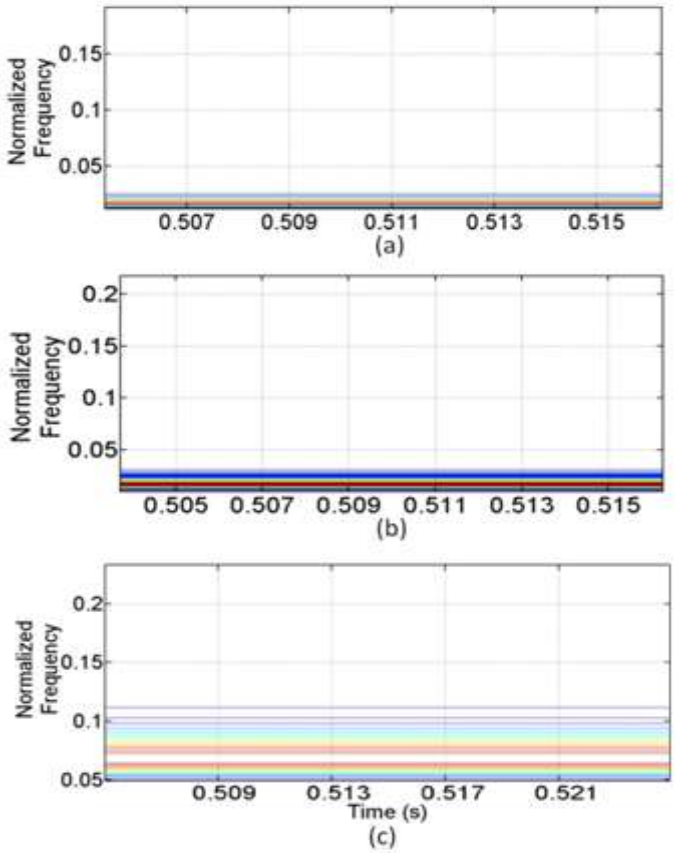

Figure 4. Spectral energy based fault classification for LG fault (a) contour for phase-R current (b) contour for phase-Y current (c) contour for phase-B current.

The time-frequency contour generated by the CWT for individual phase current (phase-R, Phase-Y, phase-B) is shown in Figure 2 (a-c). It is worth to note here that considerable variation is present in the spectral energies of phase-R and phase-B. The spectral energies E_R, E_Y, and E_B of three different phases and the difference of spectral energies between two phases for the two parts are set by a threshold value (S_{TH1}=0.085, S_{TH2}=0.07). The fault classifications of the three different phases using spectral energies are shown in Figure 3. From Figure 3, it is observed that the solid line indicates the cross-differential spectral energy ($E_{1,R}$-$E_{2,R}$) for R-phase, ($E_{1,Y}$-$E_{2,Y}$) for Y-phase, and ($E_{1,B}$-$E_{2,B}$) for B-phase. The dotted lines indicate that cross-differential spectral energy ($E_{2,R}$-$E_{1,R}$) for R-phase, ($E_{2,Y}$-$E_{1,Y}$) for Y-phase, and, ($E_{2,B}$-

$E_{1,B}$) for B-phase. It is noted that the cross-spectral energies ($E_{1,R}$ - $E_{2,R}$) and ($E_{1,Y}$ - $E_{2,Y}$) exceeds the threshold. On the contrary, the cross-spectral energies of both the PARTs such as ($E_{1,B}$ - $E_{2,B}$), ($E_{2,R}$ - $E_{1,R}$), ($E_{2,Y}$ - $E_{1,Y}$), and ($E_{2,B}$ - $E_{1,B}$) does not exceed the threshold. Therefore, the procedure explained in section 3 can be adopted and the fault in the circuit can be classified quickly and accurately. The trip signals are issued for phase-R of part-1 at t=0.542 s with the elapsed time of 13.2 ms and for phase-Y of part-1 at t=0.541 with the elapsed time of 12.9 ms.

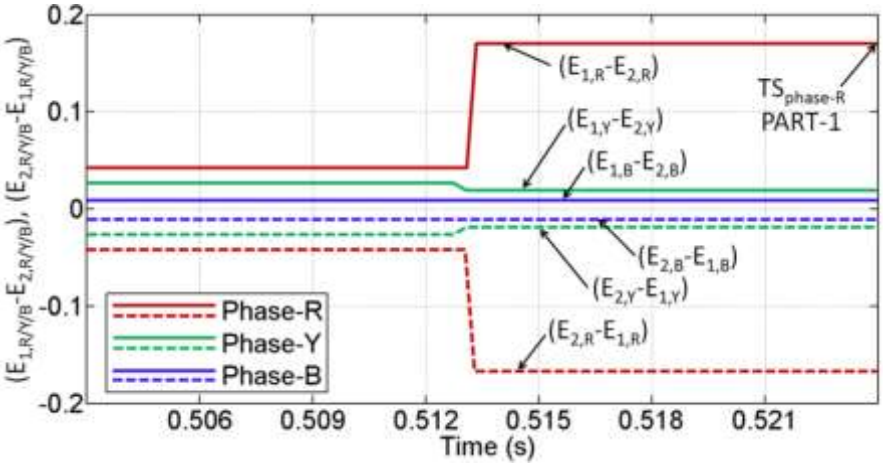

Figure 5. Fault classification on PART-2 for LG fault (a) phase-R (b) phase-Y (c) phase-B.

The spectral energies for each phase current of both the PART-1 and 2 can be calculated using the proposed CWT algorithm. To study different fault conditions the fault starts at t=0.53 s. The time-frequency contour generated by the CWT for individual phase current (phase-R, Phase-Y, phase-B) of PART-1 is shown in Figure 4 (a-c). It is noted that considerable variation is present in the spectral energies of phase-R and phase-Y. The threshold value has been set for the three different phases. The fault classification of the three different phases using spectral energies is shown in Figure 5. From Figure 5, it is observed that the solid line indicates the cross-differential spectral energy ($E_{1,R}$-$E_{2,R}$) for R-phase, ($E_{1,Y}$-$E_{2,Y}$) for Y-phase, and, ($E_{1,B}$-$E_{2,B}$) for B-phase. The dotted lines indicate that cross-differential spectral energy ($E_{2,R}$-$E_{1,R}$) for R-phase, ($E_{2,Y}$-$E_{1,Y}$) for Y-phase, and, ($E_{2,B}$-$E_{1,B}$) for B-phase. It is noted that the cross-spectral energies ($E_{1,R}$ - $E_{2,R}$) exceeds S_{TH} and the other spectral energies ($E_{1,Y}$ - $E_{2,Y}$), ($E_{1,B}$ - $E_{2,B}$), ($E_{1,B}$ - $E_{2,B}$), ($E_{2,R}$ - $E_{1,R}$), ($E_{2,Y}$ - $E_{1,Y}$), and ($E_{2,B}$ - $E_{1,B}$) does not exceed the set threshold value S_{TH}.

To study 3LG fault condition, the fault starts at t=0.525 s and one cycle of current signal is used to calculate the spectral energies of all the three phases. The time-frequency contour generated by the CWT for individual phase current (phase-R, Phase-Y, phase-B) of PART-2 is shown in Figure 6 (a-c). It is worth to note here that considerable variation is present in the spectral energies of phase-R and phase-B. It is clearly observed from Figure 7 that the cross-differential spectral energies such as ($E_{1,R}$ - $E_{2,R}$), ($E_{2,R}$ - $E_{2,R}$), ($E_{1,Y}$ - $E_{2,Y}$), ($E_{2,Y}$ - $E_{1,Y}$), ($E_{1,B}$ - $E_{2,B}$) and ($E_{2,B}$ - $E_{1,B}$) does not exceed S_{TH}. A small variation is present in phase-Y and phase-B even though it is within the set threshold limit (S_{TH}=0.085). Hence, no faulty phases have been detected in PART-1 and PART-2.

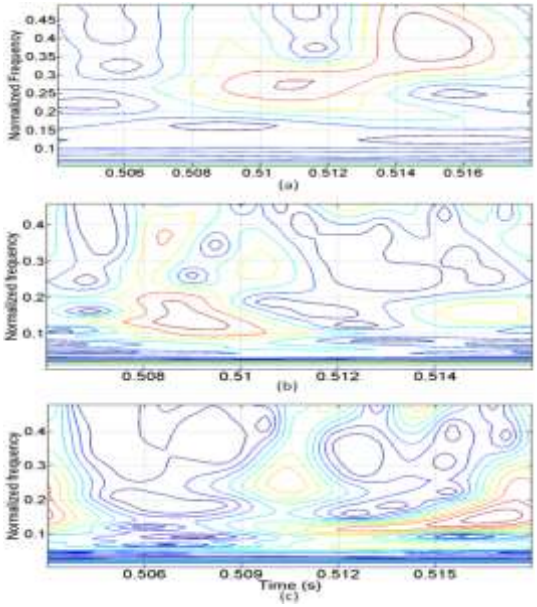

Figure 6. Spectral energy based fault classification for 3LG fault on PART-2 (a) contour for phase-R current (b) contour for phase-Y current (c) contour for phase-B current.

The CWT is applied for fault detection and classification and the proposed strategy is carried out based on the scheme provided in Figure 1. The single-phase simulation is carried out with different time inception and the CWT is applied multi-stable resonance. The fault detection is achieved if voltage of cross-disparity exceeds the set threshold value. Here the threshold values 0.85 have been set and the fault detection for LG fault is shown in Figure 8. Figure 8 illustrates that the result of LG fault (phase-Y) with fault resistance R_f=10 Ω and the fault inception time at 0.168 s. The LLG fault (phase-R and phase-Y) with fault resistance R_f=20 Ω and the fault inception time at 0.155 s is shown in Figure 9. Figure 10 depicts that the results of 3LG fault (phase-R, phase-Y and phase-B) with fault resistance R_f=10 Ω and the fault inception time at 0.148 s. From all the faults summarized, one can clearly understand that the proposed method detects the faults successfully for each phase. The proposed method uses the CWT with multi-stable resonance for improving fault detection and classification. The CWT detects the faults rapidly and improves the time detection under all the fault conditions.

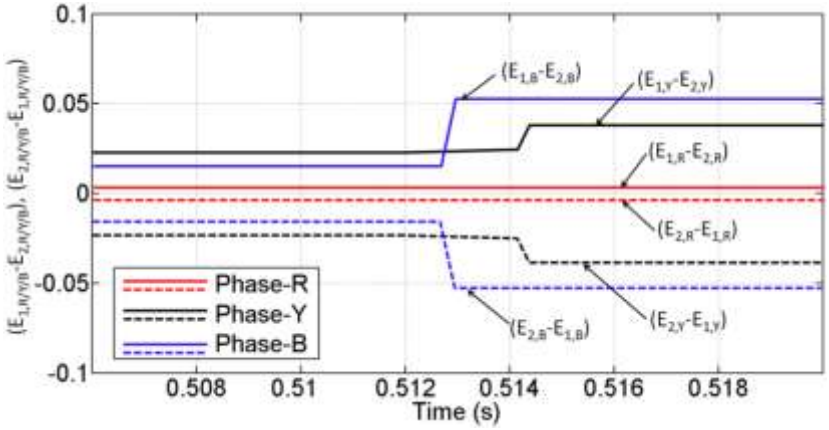

Figure 7. Fault classification using spectral energies for phase-R, phase-Y, and phase-B.

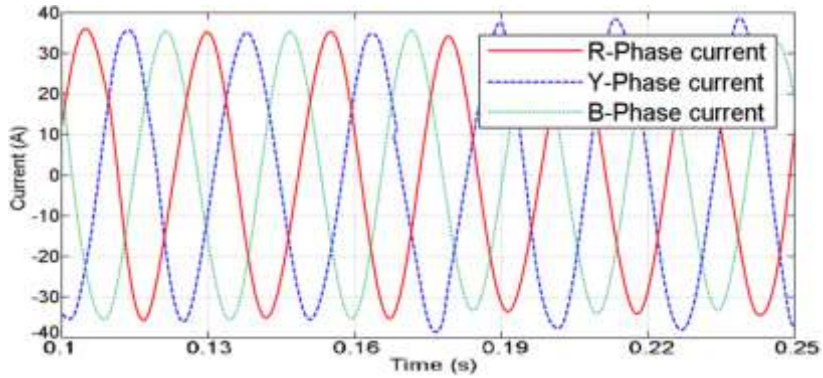

Figure 8. Transient behavior of currents under LG fault with fault resistance R_f=10 Ω.

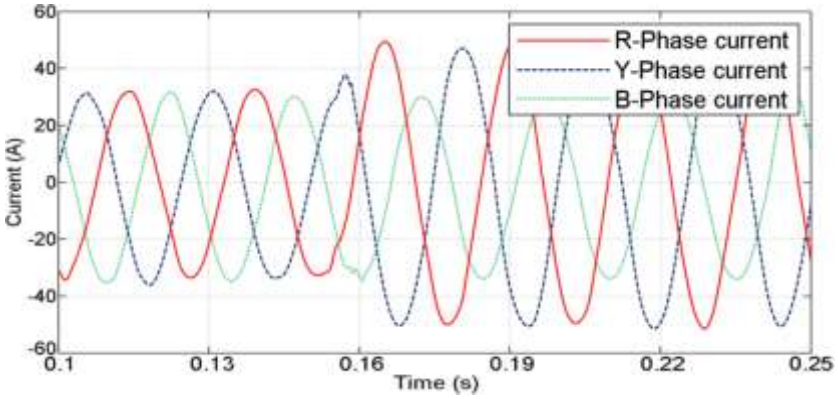

Figure 9. Transient behavior of currents under LLG fault with fault resistance R_f=20 Ω

4.2 Impact of different Faults

The fault occurs in PART-1 and PART-2 for the proposed scheme is presented in table 1. Here different fault cases has been considered for far-end of PART-1 with operating conditions such as β=90°, α=40°, $\theta_{ser} = 150^{o}$, and V_{se}=8%. The value of R_f are quit high and it is around 55 to 160 Ω. The relay response time is less than one cycle (19.25 ms) for all the three phases even the fault is considered at the far-end of transmission line. For example, the single phase fault (RG) the relay operating time is 17.56 ms and the severe RYBG fault, the operating time of relay for all the three phases are within the limits at 12.8, 13.36, and 14.63.

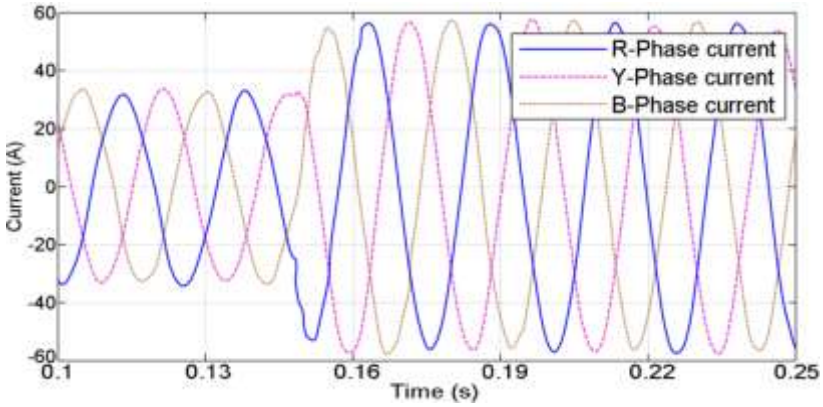

Figure 10. Transient behavior of currents under 3LG fault with fault resistance R_f=10 Ω.

The relay operating time exceeds one cycle under YBG fault case with fault location 97%. Table 2 also presents different fault cases for PART-2 with operating conditions such as β=60°, α=40°, $\theta_{ser} = 90^{o}$, and V_{se}=6%. The value of R_f is kept low and it is around 2 to 20 Ω. The fault phases decided by the proposed method have been presented in table 1. The relay response time is much less than one cycle for all the three phases even the fault is considered at the near-end of transmission line. For example, even the severe RYBG fault, the relay operating time is 10.63, 11.73, and 10.28 ms for phase-R, phase-Y, and phase-B respectively. Thus the proposed method detects the faulty phases within one cycle for all the fault cases.

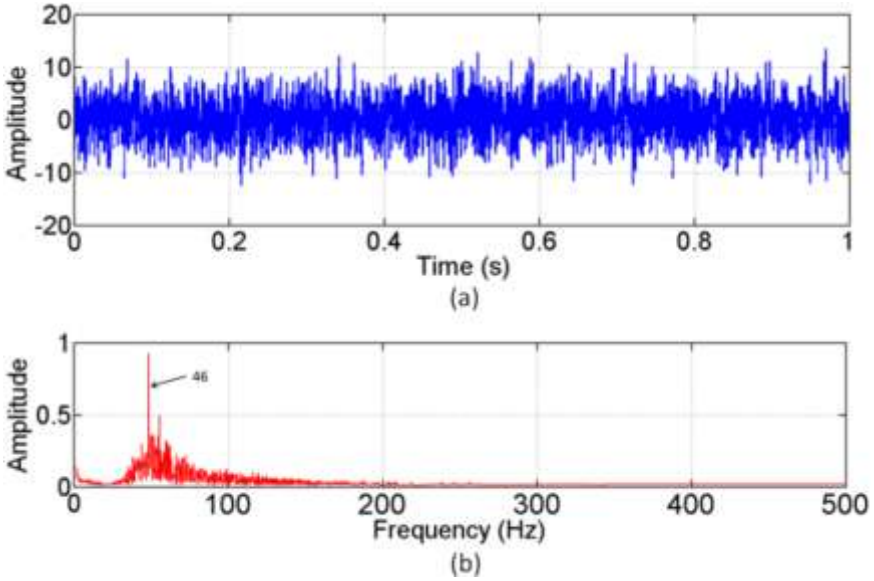

Figure 11. The simulated signal and the spectrum for EMD.

Table 1. Response of proposed method of fault detection on PART-1 and PART-2 for various faults.

Type of Fault	PART-1						PART-2					
	R_f (Ω)	Loca-tion (%)	Relay operation time (ms)			Faulted phases	R_f (Ω)	Loca-tion (%)	Relay operation time (ms)			Faulted phases
			R	Y	B				R	Y	B	
RG	105	97	17.56	-	-	R	7	12	9.47	-	-	R
YG	60	20	-	16.49	-	Y	12	15	-	9.62	-	Y
YBG	160	97	-	19.35	19.47	Y, B	20	25	-	10.37	11.62	Y, B
BRG	55	83	-	12.23	16.36	B, R	15	17	9.27	-	10.38	B, R
RY	110	72	13.14	15.45	-	R, Y	9	23	10.36	11.38	-	R, Y
B	90	78	-	16.23	12.73	Y, B	5	5	-	9.37	10.64	Y, B
BR	130	128	15.42	-	16.43	B, R	8	15	10.27	-	10.62	B, R
RYBG	105	112	12.8	13.36	14.63	R, Y, B	2	22	10.63	11.73	10.28	R, Y, B

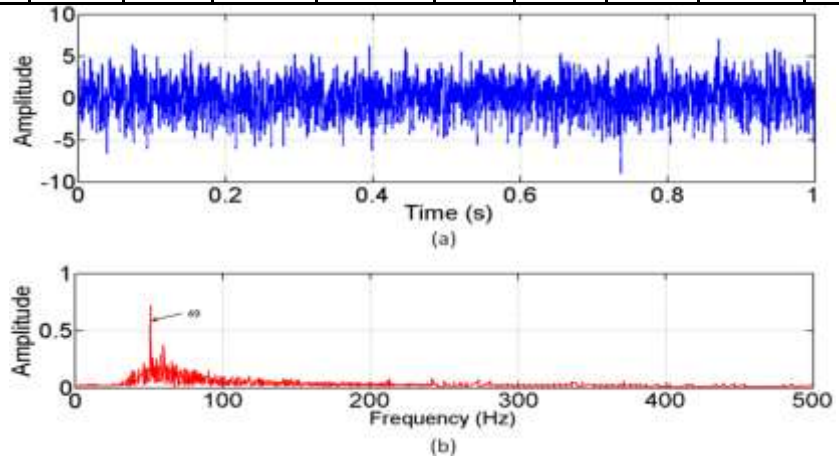

Figure 12. The simulated signal and the spectrum for WT-SAM.

The performance of the proposed method has been verified by varying the UPFC series voltage from 0% to 10% of line voltage and two different values of R_f has been considered. In this scenario different fault cases has been considered with operating conditions such as β=30°, α=40°, $\theta_{ser} = 60^o$ for PART-2. The value of R_f are quit high and it is around 55 to 160 Ω. The relay response time is within one cycle for all the three phases. The performance of phase angle of UPFC series injected voltage with different values is presented in right of table 2. The UPFC series voltage angle varies from 0 to 360° of line voltage and two different values of R_f has been considered (5 and 135 Ω). In this circumstances the operating conditions such as β=40°, α=50°, V_{se}=10 % for PART-2 has been considered. From the result one can easily understand that the proposed method identify the fault within one cycle for all the three phases and the relay operating time also within the limit (17.23 ms).

Table 2. Response of proposed method of fault detection on PART-2 for various faults with variation in V_{se} and Θ_{se}.

Variation of UPFC series injected voltage						Variation of UPFC series injected voltage phase angle					
V_{se} (%)	R_f (Ω)	Relay operation time (ms)			Faulted phases	Θ_{ser} (degrees)	R_f (Ω)	Relay operation time (ms)			Faulted phases
		R	Y	B				R	Y	B	
0	5	12.73	-	11.32	R, B	0	5	12.35	-	11.38	R, B
3	5	12.38	13.20	11.62	R, Y, B	60	5	-	11.34	12.93	Y, B
6	5	11.19	12.83	10.29	R, Y, B	180	5	-	11.67	11.73	Y, B
10	5	11.23	-	11.73	R, B	270	5	-	13.17	12.72	Y, B
0	135	14.82	14.72	-	R, Y	0	135	13.27	-	12.62	R, B
3	135	14.28	14.92	15.83	R, Y, B	60	135	-	14.35	15.82	Y, B
6	135	15.82	-	16.73	R, B	180	135	15.34	-	16.82	R, B
10	135	17.35	-	16.73	R, B	270	135	-	16.34	17.31	Y, B

4.3 Performance of Proposed method

The proposed CWT based MSR is verified in comparison with two different conventional methods: empirical mode decomposition (EMD) [27], and wavelet transform with post spectral analysis method (WT-SAM) [30]. To extract accurately the weak fault signal frequency hidden in strong noise, the above methods has been studied and compared with the proposed scheme. In this work, 19-tap symmetric bi-orthogonal filters are used at the first level after that a 14-tap linear phase complex wavelet is used. The output signal and the corresponding frequency spectrum for EMD method is shown in Figure 11. It can be seen that the output SNR of EMD is -13.645 dB. Figure 11 also shows the analyzed results of the input signal with noise intensity of 1.8.

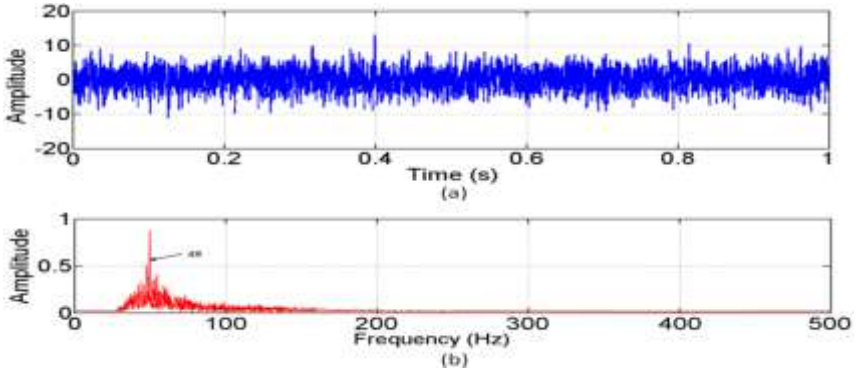

Figure 13. The simulated signal and the spectrum for the proposed method.

Table 3. The decomposition level, tuning parameter and the output SNR for EMD, WT-SAM and the proposed method.

Parameter	EMD			WT-SAM			Proposed Method		
	Decompo-sition level	Tuning parameter	Output SNR (dB)	Decomp-osition level	Tuning parameter	Output SNR (dB)	Decompo si-tion level	Tuning parameter	Output SNR (dB)
Fixed	4	12	-13.645	4	12	-11.298	4	12	-10.361
Adjustable	4	145	-10.539	4	160	-9.184	4	170	-8.640

The output signal using WT-SAM scheme and the corresponding frequency spectrum is shown in Figure 12. On comparing Figure 11 and Figure 12 it indicates that the WT-SAM method produces greater SNR than EMD method. From Figure 12 one can easily understand that the noise level is much reduced and the system SNR is relatively increased from -13.645 dB to -11.298 dB.

The output signal using CWT based MSR scheme and the corresponding frequency spectrum is shown in Figure 13. When comparing the spectrum generated by the proposed method with EMD and WT-SAM methods the output SNR of the proposed scheme increased around -3.284 dB than EMD and it is increased around -0.937 dB than WT-SAM. It is peculiar to noted that the tuning parameter is fixed, as a result non-optimal output. To obtain the optimal result of stochastic resonance, the tuning parameter β should be adjusted. The retuned value of β and the corresponding SNR and the level are listed in table 3. This result indicates the superiority and robustness of the proposed method in fault detection under high noise environment.

5. CONCLUSION

This paper presents a CWT based multi-stable resonance protection scheme for a double line transmission system including UPFC in one line. Usually the signal is buried into strong background noise and difficult to extract. The proposed method overcome the difficulty and the simulation studies has been carried out for wide operating parameters such as fault resistance, fault location, fault inception angle, and of UPFC operating parameters. The CWT based MSR scheme has been successfully applied for detection and fault classification. This approach effectively detects, classify, and locate the fault on parallel transmission system including UPFC. The location of fault can be estimated by cross-disparity of phase current. Finally, the proposed system is compared with two other conventional methods such as EMD and WT-SAM. From the results it is observed that the proposed method improve the output SNR and the accuracy of fault identification and classification. Both the simulation and performance analysis shows that the proposed CWT based MSR scheme has great potential to detect and classify the fault effectively within one cycle

References

1. Masoud Mohammadalizadeh-Shabestary, Hamed Hashemi-Dezaki, Shahed Mortazavian, Hossein Askarian-Abyaneh and Gevork Gharehpetian. A general approach for optimal allocation of FACTS devices using equivalent impedance models of VSCs. *Int Transactions on Elect Energy System*. 2014;25(7):307-1203. DOI: 10.1002/etep.1896
2. Masahide Hojo, Yasunori Mitani, Toshifumi Ise, and Kiichiro Tsuji. Quantitative evaluation of generator power control effect of FACTS controllers for power system stabilization. *Elect Engineering in Japan*. 2002;138:43-51. DOI 10.1002/eej.1127
3. Rajabi-Ghahnavieh A, Fotuhi-Firuzabad M, Shahidehpour M, Feuillet R. UPFC for Enhancing power system reliability. *IEEE Trans Power Delivery*. 2010; 25:2881-2890.
4. Wei Xuan, Chow Joe H, Fardanesh Behruz, Edris Abdel-Aty. A common modeling framework of voltage-sourced converters for load flow, sensitivity, and dispatch analysis. *IEEE Trans on Power System*. 2004;19(2):934-941.
5. Sheng-Huei Lee, Jiang-Hong Liu and Chia-Chi Chu. Modelling and locating unified power-flow controllers for static voltage stability enhancements. *Int Trans on Elect Energy System*. 2012;24(11):1524-1540. DOI:10.1002/etep.1700
6. Song Y. H. and Liu J. Y. Steady-state power flow and voltage control by unified power-flow controllers, part 1: Modelling and algorithms. *European Trans on Elect Power* 2000;10(1):53-57. DOI: 10.1002/etep.4450100108

7. Chong B X. P, Zhang K. R, Godfrey L. Yao and Bazargan M. Optimal location of unified power flow controller for congestion management. *European Trans on Elect Power.* 2010;20:600-610. DOI: 10.1002/etep.341

8. Suman Bhowmick, Biswarup Das, and Narendra Kumar. An Advanced IPFC Model to Reuse Newton Power Flow Codes. *IEEE Trans on Power System*. 2009;24:525-532. DOI: 10.1109/TPWRS.2009.2016643

9. Taher Niknam, Mohammad Rasoul Narimani, Masoud Jabbari. Dynamic optimal power flow using hybrid particle swarm optimization and simulated annealing. *European Trans on Elect Power*. 2013;23(7):975-1001. DOI: 10.1002/etep.1633

10. EI-Zonkoly AM, Desouki H. Wavelet entropy based algorithm for fault detection and classificatin in FACTS compensated transmission line. *Int J Electr Power Energy System*. 2011;33(8):1368-74.

11. He Z, Fu L, Lin S. Fault detection and classification in EHV transmission line based on wavelet singular entropy. *IEEE Trans Power Delivery*. 2010;25(4):2156-2163.

12. Dubey R, Samantaray S. R. Wavelet singular entropy-based symmetrical fault-detection and out-of-step protection during power swing. *IET Generation Transmission and Dstribution*. 2013;7(10):1123-1134.

13. Usama Y, Xiaomin L, Imam H. Design and implementation of a wavelet analysis-based shunt fault detection and identification module for transmission line aplications. *IET Generation Transmission and Distribution*. 2014;8(3):431-441.

14. Costa F.B. Fault-induced detection based on real-time analysis of the wavelet coefficient energy. *IEEE Trans Power Delivery*. 2013;29(1):140-153.

15. Benzi R, Sutera A, Vulpiana A. The mechanism of stochastic resonance. *J Phys A: Math Gen*. 1981;14(11):453-457.

16. Duan F. B, Chapeau-Blonduau F, Abbott D, Exploring weak-periodic-sugnal stochastic resonance un locally optimal processors with a Fisher information metric. *Signal Processing*. 2012;92:3049-3055.

17. He Q, Wang J, Liu Y, Dai D, Kong F. Multiscale noise tuning of stochastic resonance for enhanced fault diagnosis in rotating machines. *Mech Syst Signal Processing*. 2012;28:443-457.

18. Tao Z, Lu C, Cha Z. Multi-frequency periodic weak signal detection based on single-well potential stochastic resonance. *J Electon Meas Instrumentation*. 2014;28:171-176.

19. Mao Q, Lin M, Zheng Y. Study of weak multi-frequency signal detection based on stochastic resonance. *J Basic Sci Eng.* 2008;16:86-91.

20. Gammaitoni L, Hanggi P, Jung P, Marchesoni F. Stochastic resonance Review. *Mod Phys*. 1998;70:223-287.

21. Lie Y, Han D, Lin J. New adaptive stochastic resonance method and its application to fault diagnosis. *J Mech Eng*. 2012;48:62-67.

22. Li N, Zhou R, Hu Q, Liu X. Mechanical fault diagnosis based on redundant second generation wavelet packet transform, neighbourhood rough set and support vector machine. *Mech Sys Signal Processing*. 2012;28:608-621.

23. Riske H. The Fokker-PlancksEquation methods of solution and applications, Springer, Berlin, 1989. 1-20.

24. El-Zonkoly A.M, Desouki H. Wavelet entropy based algorithm for fault detection and classification in FACTS compensated transmission line**.** *Int J Elect Power and Energy System.* 2011;33(8):1368-1374.

25. He Q, Wang J. Effect of multi scale noise tuning on stchastic resonance for weak signal detection. *Digital Signal Processing*. 2012;22:614-621.

26. Lu S, He Q, Kong F. Sequential multi scale noise tuning stochastic resonance for train bearing fault diagnosis in an embedded system. *IEEE Trans Instrumentation and Measurement*. 2014;63:106-116.

27. He Q, Liu Y, Kong F. Machine fault signature analysis by midpoint based empirical mode decomposition. *Meas Sci Technology*. 2011;22: 015702.

28. Hrishnanand K. R, Dash P.K. A new real time fast discreate S-transform for cross differential protection for shunt compensated power system. *IEEE Trans on Power Delivery*. 2013;28(1):402-410.

29. Samantaray S. R, Tripathy L. N, Dash P. K. Differential equation-based fault locator for unified power flow controller-based transmission line using synchronized phasor measurements. *IET Generation Transmission and Distribution.* 2009;3(1):86-98.

30. Wang C, Gao R, Yan R. Unified time-scale-frequency analysis for machine defect signature extraction: Theoritical framework. *Mech Syst Signal Processing*. 2009;23:226-235.

Hari V. N, Anand C. V, Premkumar A. B, Madhukumar A. S. Design and performance analysis of asignal detector based on superthreshold stochasics resonance. *Signal Processing*. 2012;92:1745

Author's Bibliography with Photo

Mary.A.G.Ezhil received BE degree from Manonmanium Sundaranar University in 2001,ME from Bharathiar University in 2003,Currently working as assistant professor in Arunachala College of Engg. For women.Her research interests include power electronics,power systems, application of power electronics in bulk power systems.

Dr.S.JOSEPH JAWHAR, received his B.E. from Madurai amarajUniversity, M.E from Bharathiar University and Ph.D from Anna University in 2009. He is currently working as Professor in Electrical and Electronics Engineering Department at Arunachala College ofEngineering for Women, Vellichanthai. Hehas presented number of papers in various national and International conferences and published number of papers in reputed international journals. His research interests include power electronics, real-time control systems, soft computing techniques and electrical drives.

C. Chellaswamy, obtained his bachelor'sdegree in Electronics and Communication Engineering from Madurai Kamaraj University, India and M.Ein Applied Electronics from Sathyabama University, Chennai, Tamilnadu, India in 1994 and 2005respectively. He is currently working as Associate Professor at Rajalakshmi Institute of Technology, Chennai. He has presented number of papers in various national and International conferences and published number of papers in international journals. His current fields of interest are VLSI Signal processing, Implementation of new systems and System Design using Micro Controller.